Nuclear Instruments and Methods in Physics Research A 783 (2015) 43–50

Contents lists available at ScienceDirect

Nuclear Instruments and Methods in Physics Research A

journal homepage: www.elsevier.com/locate/nima

Influence of wavelength-shifting films on multianode PMTs with UV-extended windows

J. Adamczewski-Musch [a], K.-H. Becker [b], S. Belogurov [c], N. Boldyreva [d], A. Chernogorov [c], C. Deveaux [e], V. Dobyrn [d], M. Dürr [e,*], J. Eom [f], J. Eschke [a], C. Höhne [e], K.-H. Kampert [b], V. Kleipa [a], L. Kochenda [d], B. Kolb [a], J. Kopfer [b,**], P. Kravtsov [d], S. Lebedev [e], E. Lebedeva [e], E. Leonova [d], S. Linev [a], T. Mahmoud [e], J. Michel [g], N. Miftakhov [d], Y. Nam [f], W. Niebur [a], K. Oh [f], E. Ovcharenko [c], C. Pauly [b], J. Pouryamout [b], S. Querchfeld [b], J. Rautenberg [b], S. Reinecke [b], Y. Riabov [d], E. Roshchin [d], V. Samsonov [d], J. Song [f], O. Tarasenkova [d], T. Torres de Heidenreich [a], M. Traxler [a], C. Ugur [a], E. Vznuzdaev [d], M. Vznuzdaev [d], J. Yi [f], I.-K. Yoo [f]

[a] GSI Helmholtzzentrum für Schwerionenforschung GmbH, D-64291 Darmstadt, Germany
[b] Department of Physics, University Wuppertal, D-42097 Wuppertal, Germany
[c] SSC RF ITEP, 117218 Moscow, Russia
[d] PNPI RAS Gatchina, 188300 Gatchina, Russia
[e] Institute of Physics II, Institute of Applied Physics, Justus Liebig University Giessen, D-35392 Giessen, Germany
[f] Department of Physics, Pusan National University, 609-735 Pusan, Republic of Korea
[g] Institut für Kernphysik, Goethe University Frankfurt, D-60438 Frankfurt am Main, Germany

ARTICLE INFO

Article history:
Received 24 November 2014
Received in revised form
4 February 2015
Accepted 5 February 2015
Available online 14 February 2015

Keywords:
Wavelength-shifting films
Dip-coating
Multianode PMT
Quantum efficiency
Cherenkov detector
RICH

ABSTRACT

Wavelength-shifting (WLS) films were applied on UV-extended front windows of multianode photomultiplier tubes (MAPMTs) in order to increase the sensitivity of the MAPMTs at shorter wavelengths. The WLS material contained p-Terphenyl as photoactive component, which absorbs shorter wavelength photons (<300 nm) and re-emits fluorescence photons around 350 nm, i.e., at the maximum of the PMTs' sensitivity. The films were applied by means of dip-coating and the film performance was studied with respect to quantum efficiency, film homogeneity, and crosstalk on the MAPMTs. Using WLS-film-covered MAPMTs in a gaseous Ring Imaging Cherenkov detector, the number of detected photoelectrons per ring increased by up to 21% in an in-beam test.

1. Introduction

For the application in Cherenkov detectors, the sensitivity of photomultiplier tubes (PMTs) is requested to cover a wide range of the electromagnetic spectrum from the visible to the UV region. For long wavelengths, the spectral sensitivity of PMTs is limited by the photocathode material itself. At wavelengths $\gtrsim$600 nm, the photon energy is too low to overcome the work function of the (bialkali) photocathode of approximately 2 eV [1]. In the short wavelength region, the reduced transparency of the PMT front windows for UV light is the main limiting factor. While the transparency of standard borosilicate glass is strongly reduced below $\approx$300 nm, this limit is shifted to $\approx$220 nm in the case of UV-extended windows, and to $\approx$180 nm in the case of quartz windows [2]. Given the behavior of the Cherenkov spectrum (the total number of photons is proportional to $1/\lambda$), the short wavelength limit is of particular importance when using PMTs in Cherenkov detectors: the more sensitive the photon detector is for short-wavelength Cherenkov photons, the larger is the integrated photon yield. For gaseous Cherenkov detectors, the short wavelength cutoff is given by the radiator gas; e.g., $\approx$185 nm for CO_2

* Corresponding author.
** Corresponding author.
E-mail addresses: michael.duerr@ap.physik.uni-giessen.de (M. Dürr), kopfer@uni-wuppertal.de (J. Kopfer).

http://dx.doi.org/10.1016/j.nima.2015.02.014
0168-9002/

[3] as foreseen as radiator for the Ring Imaging Cherenkov (RICH) detector of the Compressed Baryonic Matter (CBM) experiment at the future Facility for Antiproton and Ion Research (FAIR) [4,5]. It is, therefore, beneficial to design the photon detector in such a way that it is sensitive to these wavelengths as long as the loss of spatial resolution due to the more pronounced chromatic dispersion at shorter wavelengths is tolerable.

One way to extend the short-wavelength limit of PMTs is the use of wavelength-shifting (WLS) films applied to the PMT front window. WLS films are typically made from organic molecules, which absorb light in the UV region and re-emit fluorescence photons at larger wavelength, ideally in the wavelength region of the maximum spectral sensitivity of the photocathode material in use. The WLS technique has been proposed already in 1973 by Garwin and coworkers for PMTs with standard glass window used in gaseous Cherenkov detectors [6]. WLS films on top of small-scale photon detectors with standard glass as an alternative to more expensive devices with, e.g., quartz, LiF, MgF_2, or GaF_2 windows, have been discussed and applied in the following [7–12]. A significant time delay is not associated with the use of WLS films: for p-Terphenyl (PT) as used in this study, a fluorescence decay time of the order of a few nanoseconds was reported [7,13].

The use of WLS films on PMTs with an UV-extended window is less favorable when compared to PMTs with standard borosilicate window due to the relatively high transparency of UV-extended glass in the UV-region. Furthermore, when using WLS films on PMTs with segmented anode and dynode structures, so-called multianode PMTs (MAPMTs), crosstalk between neighboring pixels due to the isotropic fluorescence of the WLS films has to be considered.

In this paper, we report on an comprehensive study of the performance of WLS films on MAPMTs with UV-extended windows. With respect to the application of the WLS films, we focus on dip-coating which is an inexpensive process and allows for covering large surface areas with homogeneous layers. In addition, dip-coating layers containing a binder material are mechanically more robust than, e.g., vacuum-deposited WLS films. For the photoactive substance in the film, we restrict ourselves to PT, which was shown to exhibit superior performance as WLS material on PMTs when compared to other standard WLS substances such as tetraphenyl-butadiene [14]. Measurements of quantum efficiency *QE* as a function of wavelength were performed with and without WLS films to study the influence of the WLS films in the different wavelength regions. Especially the influence of film thickness was investigated as it turns out to be of particular importance in the case of PMTs with UV-extended windows. Crosstalk between the single channels of MAPMTs covered with WLS films was also quantified as it is expected to be affected by the isotropic emission of fluorescence photons in the WLS film. Furthermore, *QE* measurements of different types of MAPMTs with and without WLS film are presented; the effect of WLS films on MAPMTs with UV-extended windows used in a RICH detector is discussed based on results of an in-beam test at the CERN PS T9 beam line.

2. Experimental techniques

2.1. Sample preparation

We applied the WLS films by dip-coating the MAPMT windows from a solution consisting of 15 g/L PT ($>99\%$, Alfa Aesar, Karlsruhe, Germany) as photoactive substance and 24 g/L paraloid B72 (Carl Roth GmbH, Karlsruhe, Germany) as binder dissolved in dichloromethane (99.5%, Carl Roth GmbH, Karlsruhe, Germany). Paraloid B72 is the commercial name of a binary copolymer of methyl acrylate and ethyl methacrylate with low absorption in the interesting wavelength region and good ageing properties [15]; it is abbreviated paraloid in the following. The MAPMTs are dipped into the solution with their front window perpendicular to the solution's surface and are then pulled out of the solution at constant speed. In order to expose only the front window to the solution and to protect the MAPMTs, a tight housing was used for the MAPMTs during the dipping process. In order to further characterize the respective layers, dip-coated films were also applied on quartz substrates of 1 mm thickness using the same set-up. Pulling speed was chosen between 10 cm/min and 65 cm/min relative to the surface of the solution; however, reproducible results were obtained only for a pulling speed up to ≈ 40 cm/min, for higher pulling speed evaporation of dichloromethane was too slow for a reproducible formation of homogeneous films. The higher the pulling speed, the thicker the applied films; in the range between 10 cm/min and 40 cm/min a mean film thickness between 50 and 200 nm was achieved as determined by means of scanning electron micrographs of the film profiles [compare Fig. 1(a) and (b)]. Towards higher layer thickness, the roughness of the layers' surface also increases; in the inset of Fig. 2, the error bars indicate minimum and maximum thickness of the respective layers. For comparison, one MAPMT was covered by means of evaporating crystalline PT from a molybdenum boat which was heated resistively up to 200 °C in a vacuum evaporator. The evaporated film was 1 μm thick [14].

2.2. Characterization methods

The WLS films were characterized in terms of photon absorption and fluorescence as well as quantum efficiency and Cherenkov photon detection efficiency using the following methods:

(a) Absorption and fluorescence measurements – Absorption measurements were performed in solution and of films on quartz substrates using a UV-vis absorption spectrometer (Lambda 35, Perkin Elmer); fluorescence spectra were recorded in a 90° set up (excitation beam/fluorescence detection) both for solution and films using a standard fluorescence spectrometer (Cary Eclipse, Agilent Technologies).

(b) Quantum efficiency measurements – For measuring the *QE* of MAPMTs coated with WLS films, the first three dynodes were shorted and the photocurrent from the photocathode was measured by a picoamperemeter while illuminating the photocathode with monochromatic light. A potential of -100 V was applied between photcathode and dynode system in order to collect all photoelectrons. A deuterium-tungsten-halogen hybrid light source was utilized in order to cover the wavelength range between 200 nm and 750 nm. A double grating monochromator was used to select wavelengths in steps of 10 nm in combination with longpass filters to suppress higher orders in the diffraction pattern of the gratings. Given a constant illumination, the *QE* of the MAPMT could be determined with a subsequent measurement of a calibrated photodiode. The *QE* was calculated as ratio of the photocurrents of the MAPMT and that of the photocathode multiplied by the *QE* of the calibrated photodiode. The dark current of the MAPMTs was measured after storing them in darkness and was considered in the calculation. The overall measurement error is given by the uncertainty of the photodiode calibration and that of the picoamperemeter adding up to 5–10%. The *QE* of every MAPMT was measured as a function of wavelength between 200 nm and 750 nm (*QE* curve); in order to compare their performance in the UV region, the measurements of dip-coated and bare MAPMTs were performed with the same photodetector unless stated otherwise. When the measurement of the bare MAPMT was performed after the measurement of the coated one, the WLS film was wiped off the PMT window using dichloromethane and a soft tissue. In addition, *QE* was measured as function of position on the MAPMT front window (*QE* scan) by

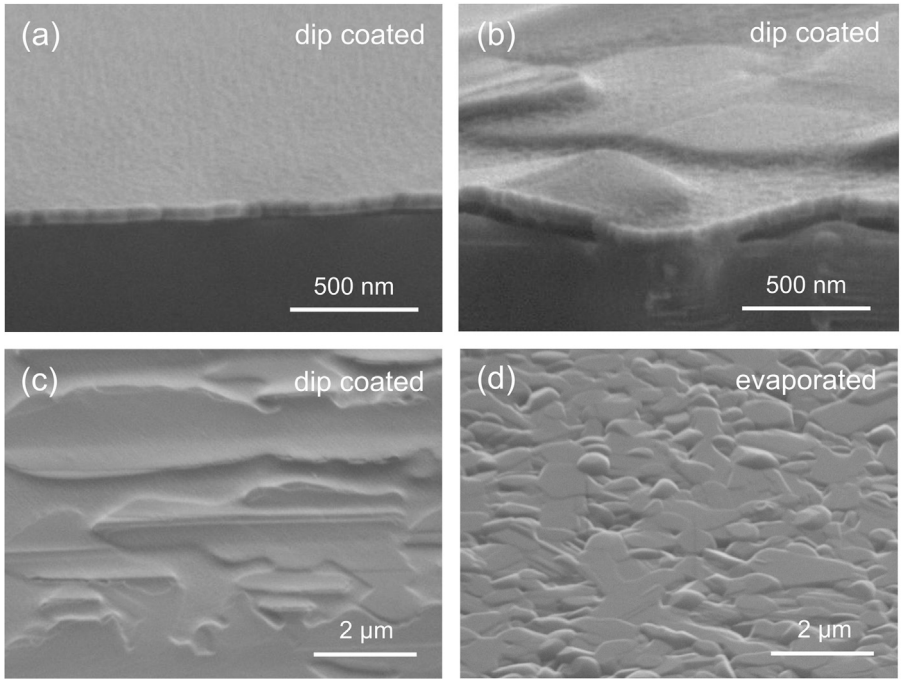

Fig. 1. Scanning electron micrographs in bird's eye view (top: 60° off normal, bottom: 30° off normal) of dip-coated PT/paraloid films with a thickness of (a) 50 nm, (b) and (c) 100 nm, and (d) evaporated PT layer.

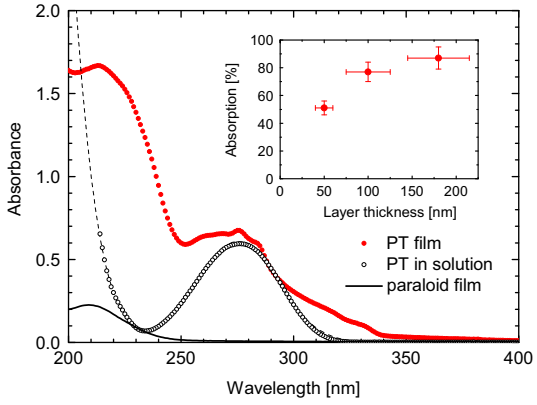

Fig. 2. Absorbance of a PT/paraloid film (180 nm) on a quartz substrate measured as a function of wavelength (background-corrected, red dots). For comparison, the absorbance of PT in dichloromethane (4 mg/L, open dots) and of paraloid on quartz (coated from a pure paraloid solution, 24 g/L in dichloromethane, straight line) is shown. Inset: Absorption measured at 220 nm for three films of different thickness, error bars indicate the roughness of the respective films. (For interpretation of the references to color in this figure caption, the reader is referred to the web version of this article.)

using a light fiber and a pinhole resulting in a spot size <1 mm in diameter.

(c) Single-photon scans – Due to the isotropic fluorescence of WLS films, the amount of crosstalk between neighboring pixels is affected when using WLS films on MAPMTs. We determine crosstalk on a single-photon level which is the meaningful quantity with respect to gaseous Cherenkov detectors that measure single Cherenkov photons. In order to quantify the crosstalk between neighboring pixels of a MAPMT, a position sensitive measurement with single photons was performed (single-photon scans). For this purpose, light pulses from LEDs of 245 nm and 470 nm were geometrically attenuated and coupled into a UV-transparent light fiber. By using a pinhole mask at the end of the fiber, which was connected to an xy-stage, single-photon illumination of MAPMTs with a spatial precision <1 mm could be achieved. For comparison of the crosstalk with and without WLS films, a MAPMT with WLS film was used and the film was wiped off (see above) before measuring the bare MAPMT.

Table 1
Characteristics of the tested MAPMT types. All MAPMTs have a quadratic front window made from UV-extended glass. The Hamamatsu nomenclature is "−03" for UV-extended window plus bialkali (BA) photocathode and "−103" for UV-extended window plus super bialkali (SBA) photocathode. All three MAPMT types have a pixel size of 5.8×5.8 mm^2.

MAPMT type	Side length (mm)	Window thickness (mm)	Photocathode	No. of dynodes
R11265-103-M16	26.2	0.8	SBA	12
H8500D-03	52.0	1.5	BA	12
H10966A-103	52.0	1.5	SBA	8

(d) In-beam test – The performance of dip-coated WLS films for the detection of Cherenkov rings was tested with the CBM RICH prototype detector at the CERN PS T9 beamline [5,16]. This prototype detector consists of a 1.7 m long CO_2 gas radiator at atmospheric pressure, a UV-reflecting spherical mirror of 3 m radius of curvature, and a photon detector consisting of approximately 20 MAPMTs. During the beam test, a mixed beam of electrons, pions, and muons at momenta between 2 GeV/c and 10 GeV/c entered the detector box causing a Cherenkov cone, which was projected by a mirror onto the photon detector. By tilting the mirror, the projected Cherenkov rings could be focussed on different parts of the photon detector. Since electrons are ultrarelativistic in the available momentum range, electron rings are saturated, i.e., their radius and hit multiplicity is momentum independent. Therefore, electron rings, which were selected by using two threshold Cherenkov counters installed in the beam line, were used exclusively for the data analysis discussed below.

The photon detector itself consisted of H8500D-03, H10966A-103, and R11265-103-M16 MAPMTs (Hamamatsu Photonics K.K., Hamamatsu, Japan, compare Table 1). The Cherenkov ring radius is approximately 45 mm so that one ring fits on an array of four

2×2 in.^{2} MAPMTs. For the in-beam test, the MAPMTs were dip-coated with WLS films. In order to determine the performance of the films, Cherenkov rings were projected onto the coated MAPMTs. The films were then removed and subsequent reference measurements were performed without films. Radiator temperature and pressure were monitored in order to correct for variations of the refractive index.

3. Results

3.1. Absorption and fluorescence

Fig. 2 shows the light absorption of an approximately 180 nm thick PT / paraloid film as a function of wavelength that was prepared with the dip-coating techniques on a quartz substrate. The absorbance of the film, i.e., $\ln(I_0/I)$ with I_0 being the incoming light intensity and I being the transmitted light intensity, is compared to the absorbance of PT in dichloromethane and a pure paraloid film. In solution, absorption occurs below 300 nm with a local minimum around 230 nm. In the film, the first maximum is also found around 270 nm but the second peak is shifted towards longer wavelengths and both peaks are broadened when compared to PT in solution. The film is transparent above 350 nm; paraloid shows only a minor absorbance in the wavelength range of interest. In the inset of Fig. 2, the absorption, $(I_0-I)/I_0$, measured at 220 nm is summarized for three layers of different thickness; saturation towards the thicker layers is observed.

Fig. 3 shows the fluorescence of PT films when excited with UV photons of 230 nm as a function of wavelength. Fluorescence intensity spreads from 325 nm to 425 nm and, therefore, matches the wavelength region of maximum *QE* of BA and SBA photocathodes very well (see below). With increasing layer thickness, fluorescence intensity increases but saturates for the thickest layer. This is in accordance with the absorption spectra, which indicate that in the maximum of absorption around 220 nm almost all photons are absorbed at the given layer thickness.

3.2. The QE of MAPMTs with UV-extended window—influence of film thickness

Fig. 4 (top) shows the *QE* curves of a H8500-03 MAPMT with and without an evaporated PT film of 1 μm thickness. The H8500-03 MAPMT is an older version of the H8500D-03 model. Both MAPMT types have the same characteristics relevant for this study as listed in Table 1. The influence of the WLS film is different in three different wavelength regions: (a) for wavelengths below

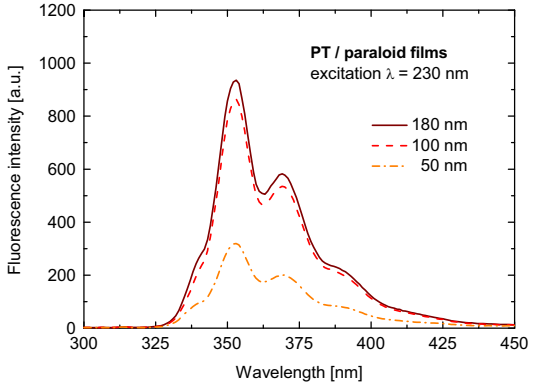

Fig. 3. Fluorescence intensity as a function of wavelength for 3 layers of different film thickness measured with an excitation wavelength of 230 nm. The maximum of fluorescence matches the wavelength range of maximum quantum efficiency of BA and SBA photocathodes.

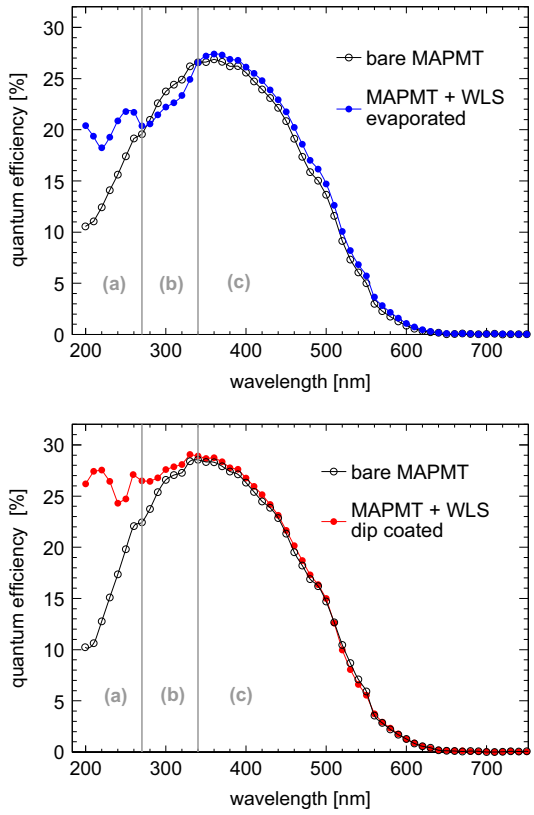

Fig. 4. Top: *QE* curves of uncoated and coated H8500-03 MAPMT with an evaporated WLS film of 1 μm thickness. The vertical lines separate three wavelength regions with increased *QE* below 270 nm (a), lower *QE* between 270 nm and 340 nm (b), and increased *QE* above 340 nm (c) of the WLS coated MAPMT when compared to the uncoated one. Bottom: *QE* curves of uncoated and coated H8500-03 MAPMT with dip-coated WLS film of ≈180 nm thickness.

270 nm, the *QE* is higher for MAPMTs with WLS-film coating than that for bare MAPMTs; (b) for wavelengths between 270 nm and 340 nm, the *QE* of MAPMTs with WLS-film coating is reduced compared to the bare MAPMTs; (c) for wavelengths above 340 nm, the *QE* is again higher for MAPMTs with WLS-film coating than that of the bare MAPMTs. The efficiency increase in region (a) is due to shifting the UV photons to a wavelength for which the *QE* of the MAPMT is higher. In region (b), the efficiency decrease is caused by the overlap of the absorption range of PT with the wavelength range where the bare MAPMT is also sensitive (cf. Fig. 2). This overlap is much less pronounced for standard borosilicate windows with a higher cutoff wavelength for QE_{bare} around ≈300 nm as determined by the transparency of the borosilicate glass [14]. The slight efficiency increase in *QE* in region (c) is attributed to a better light harvesting mainly based on scattering in the evaporated WLS films [11,12].

For comparison, Fig. 4 (bottom) shows the *QE* results of a bare and dip-coated MAPMT H8500D-03 (layer thickness 180 nm). Both in region (a) and (b), the *QE* is higher for MAPMTs with WLS-film coating than that of bare MAPMTs. Apparently, the layer is sufficiently thin, so that absorption in region (b) plays a minor role but is still sufficiently thick to ensure a strong increase of the *QE* in region (a); indeed for wavelengths between 200 nm and 400 nm, the *QE* is almost constant. The *QE* curves with and without WLS film were measured with three layers of different thickness as those used for the measurements of the fluoresce spectra shown in Fig. 3. Since the *QE* curves of the bare MAPMTs differ significantly, a direct quantitative comparison of WLS films of different MAPMTs is difficult. Therefore, the difference between *QE* with and without WLS films is normalized to maximum *QE* of

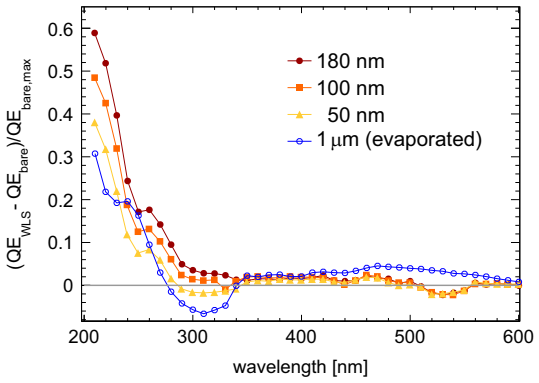

Fig. 5. Difference of *QE* between WLS coated and uncoated MAPMTs normalized to maximum *QE* of the uncoated MAPMTs. The normalization allows for a better comparison of the films since different MAPMTs have different *QE*. An increase of relative gain with increasing film thickness of the dip-coated films from 50 to 180 nm can be observed. For comparison, the relative gain of an evaporated WLS film of 1 μm thickness is also plotted. The lower quantum efficiency between 270 nm and 340 nm with evaporated WLS film translates into negative gain values.

the bare MAPMT according to $(QE_{\mathrm{WLS}}-QE_{\mathrm{bare}})/QE_{\mathrm{bare,max}}$. We refer to this normalized difference in *QE* in the following as *relative gain*. A positive (negative) relative gain indicates higher (reduced) *QE* for MAPMTs with WLS-film compared to that of bare MAPMT. Fig. 5 shows the relative gain for MAPMTs with three dip-coated layers and a MAPMT that was coated with PT by means of evaporation. For all dip-coated layers, a significant increase in *QE* for wavelengths $\lambda \leq 300$ nm is observed. Within the series of dip-coated layers, the normalized gain increases with increasing layer thickness up to the thickest layer of 180 nm.

In comparison to the dip-coated films, the MAPMT with evaporated WLS layer shows an in general lower increase in *QE* for $\lambda \leq 280$ nm. Additionally, a pronounced decrease in *QE* between 280 and 340 nm is observed due to absorption of PT (compare also Figs. 2 and 4). No significant decrease in this wavelength region is observed for the much thinner dip-coated layers. For 400 nm $\leq \lambda \leq$ 600 nm, the evaporated layer shows a slight increase in *QE* in contrast to the dip-coated layers. This increase is mainly attributed to light scattering in the evaporated film [11,12] as the evaporated films appear more opaque when compared to the dip-coated layers. The increased scattering strength of the evaporated film is first caused by the larger layer thickness (1 μm versus $\leq$ 200 nm) and might be enhanced by the formation of crystals on the (sub-)micron scale in the evaporated films as observed in the SEM images (Fig. 1(d)).

One might speculate on an even higher relative gain for a layer thickness between 200 nm and 1 μm, a thickness region not accessible with our dip-coating process. However, based on our experimental results, especially the saturation behavior observed in the thickness dependent absorption and fluorescence measurements (see Figs. 2 and 3), as well as from the comparison of absolute *QE* values measured between 200 and 300 nm with the maximum *QE* value around 350 nm, no significant further increase in *QE* towards thicker layers is expected.

3.3. Dip-coated WLS films on different MAPMT types

In order to study the effect of dip-coated WLS films on different types of MAPMTs, WLS films of $\approx$200 nm thickness were applied on three MAPMTs with different thickness of the UV-glass window and different photocathode materials (Table 1).

Fig. 6 shows *QE* curves (top) and the corresponding relative gain (bottom) for the different MAPMT types. A hierarchy of gain in *QE* of the coated with respect to the uncoated MAPMTs in the UV wavelength region can be seen. The difference in gain is

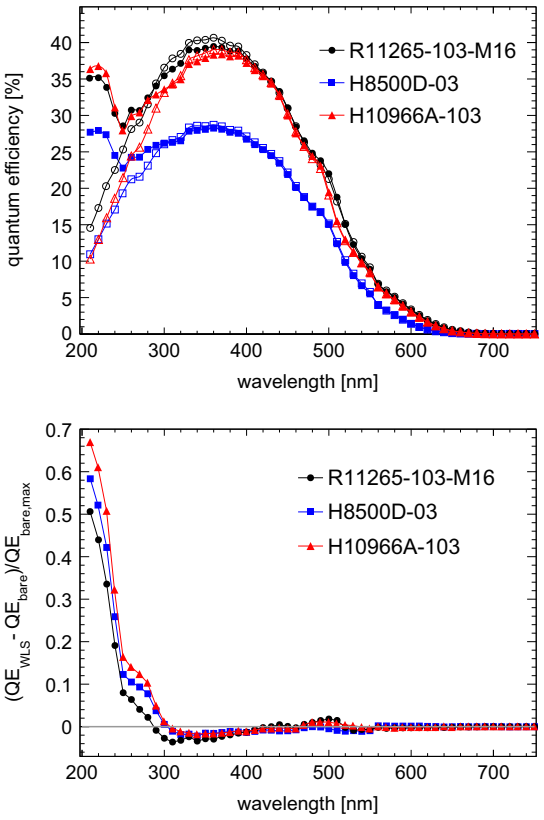

Fig. 6. Top: *QE* curves of R11265-103-M16, H8500D-03, and H10966A-103 MAPMTs without (open symbols) and with dip-coated WLS films ($\approx$ 200 nm, full symbols). The curves for R11265-103-M16 and H8500D-03 show the average *QE* from four MAPMTs, the curve for H10966A-103 represents data from the measurement of one single MAPMT. Bottom: Relative gain of WLS coated compared to uncoated MAPMTs. A hierarchy of performance gain achieved by the WLS coating for the different MAPMT types can be clearly observed (see main text for explanation).

determined both by photocathode material and window thickness. For SBA photocathodes, the gain is larger than that of BA photocathodes since MAPMTs with SBA photocathodes have a higher *QE* in the region the UV photons are shifted to than MAPMTs with BA photocathodes. In addition, MAPMTs with thinner front windows (0.8 mm) have a lower gain than those with thicker front windows (1.5 mm). A thinner front glass exhibits a better UV transmittance already leading to a higher *QE* at lower wavelengths without any WLS films

As a consequence, the relative gain observed for the H10966A-103 (SBA, 1.5 mm) is higher than the one observed for the H8500D-03 (BA, 1.5 mm). When comparing MAPMTs with the same photocathode, the R11265-103-M16 with the thinner window (0.8 mm) exhibits a smaller relative gain than that of the H10966A-103 with thicker front window (1.5 mm).

3.4. Film homogeneity

Fig. 7 (top) displays *QE* scans at 240 nm and 470 nm of one H8500D-03 MAPMT with dip-coated WLS film ($\approx$ 200 nm) on the whole front window. In addition, the *QE* scans of the bare MAPMT are shown (Fig. 7 (bottom)). Strongly enhanced *QE* at 240 nm and relatively unchanged *QE* in the visible wavelength region can be observed for the whole surface. Both the dip-coated as well as the evaporated WLS film (results not shown) do not show any remarkable structures or regions with low *QE*. In contrary, a very homogeneous spatial *QE* distribution can be observed.

In order to quantify the WLS film homogeneity, the difference between maximum and minimum *QE* on the MAPMT surface at a

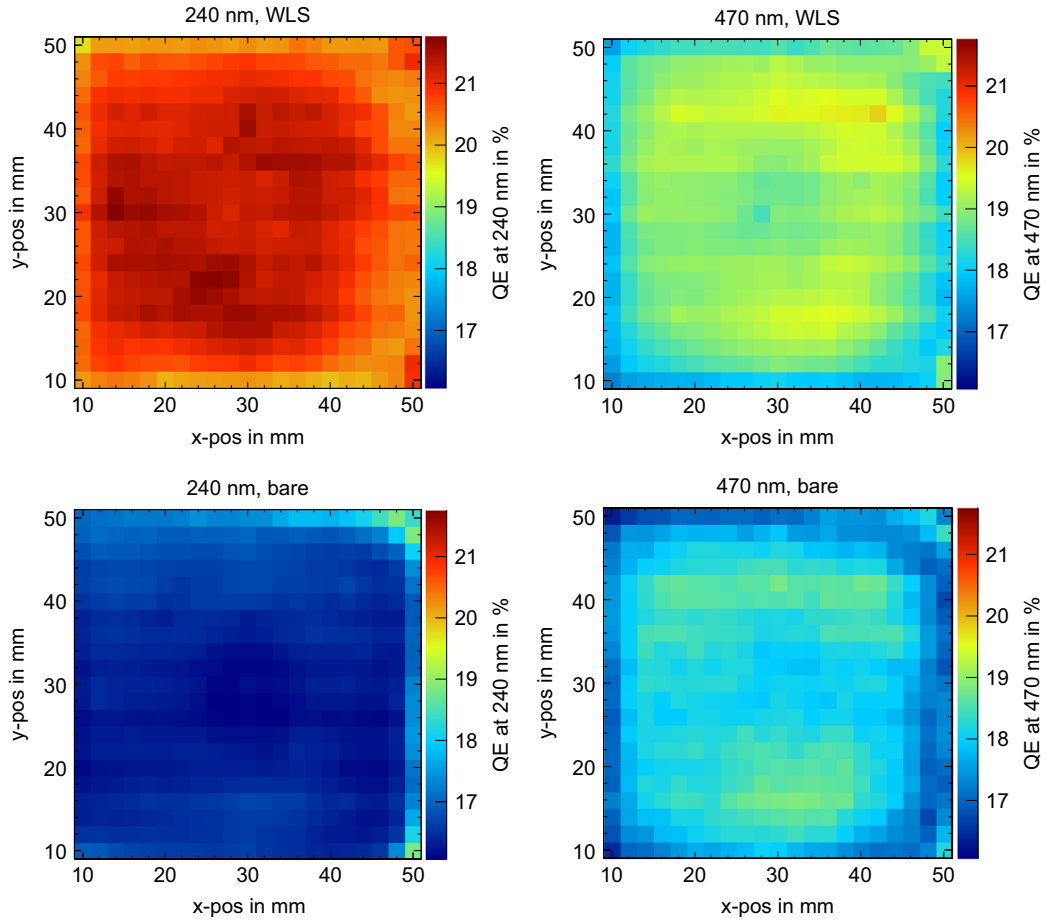

Fig. 7. *QE* scans of a H8500D-03 with (top line) and without (bottom line) dip-coated WLS film (≈ 200 nm) at 240 nm (left column) and 470 nm (right column) illumination.

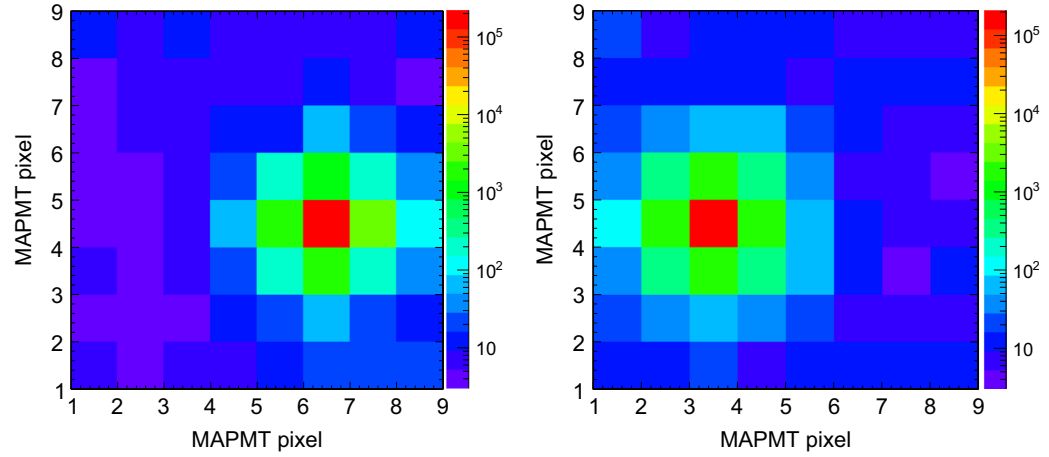

Fig. 8. Number of hits per pixel for the illumination of the central 5×5 mm^2 of an uncoated (left) and a WLS coated pixel (right) with single photons. More crosstalk is observed in the neighboring pixels when using WLS films. Note the logarithmic scale of the color coding. (For interpretation of the references to color in this figure caption, the reader is referred to the web version of this article.)

given wavelength normalized to the maximum value is calculated:

$$h = \frac{QE_{\max} - QE_{\min}}{QE_{\max}}. \quad (1)$$

With this definition, h is a measure for the variation of *QE* over the MAPMT surface. Since *QE* of the bare MAPMTs varies over the surface due to the MAPMT production process, h_{WLS} of the coated MAPMT is compared to h_{bare} of the bare MAPMT. The normalized difference Δh_{norm} between h_{WLS} and h_{bare},

$$\Delta h_{\mathrm{norm}} = \frac{h_{\mathrm{WLS}} - h_{\mathrm{bare}}}{h_{\mathrm{bare}}}, \quad (2)$$

gives then an estimate of the homogeneity of WLS films. For the WLS film shown in Fig. 7, the decrease in homogeneity from uncoated to coated MAPMT was determined to be $\Delta h_{\mathrm{norm}} = 36\%$.

3.5. Crosstalk – charge sharing

Crosstalk is defined here in the sense of charge sharing between neighboring pixels in the following way: we illuminated the central 5×5 mm^2 of a MAPMT pixel with single photons from a pinhole. The hits in the illuminated as well as in the adjacent pixels were detected. The crosstalk is then defined by the number of hits in adjacent pixels normalized to the number of hits in the illuminated pixel.

Fig. 8 shows the number of hits as a function of the MAPMT pixel position for the illumination of the central 5×5 mm^2 of one pixel. In the left plot, an uncoated pixel and in the right plot a pixel coated by a WLS film was illuminated. An enhanced crosstalk is observed in the right plot, especially in the diagonal neighbors.

Table 2 shows the crosstalk in next neighboring pixels measured for one and the same H8500D-03 MAPMT with and without WLS films. To quantify the overall crosstalk, we consider hits in the next as well as in next-to-next neighboring pixels. Without film, the crosstalk adds up to 3.8% at 470 nm and also 3.8% at 245 nm. For WLS coated pixels, the crosstalk is 3.8% at 470 nm and 4.7% at 245 nm. These numbers show that at 470 nm, a wavelength at which the WLS film is transparent, crosstalk is comparable with and without coating. At 245 nm, however, the crosstalk is larger by 24% with WLS coating due to the isotropic fluorescence of the film. The influence of crosstalk from WLS films on the Cherenkov ring sharpness will be discussed in the next section.

Table 2
Crosstalk of an uncoated (left) and a different but coated (right) pixel of a H8500-03 MAPMT illuminated at 245 nm (top) and 470 nm (bottom). The charge detected in the pixels in the direct neighborhood of the center pixel (CP) is given in percent with respect to the charge detected in the center pixel (=100%).

uncoated, 245 nm

0.1	0.6	0.1
0.8	CP	1.1
0.1	0.7	0.1

coated, 245 nm

0.2	0.7	0.2
1.1	CP	1.0
0.2	0.8	0.1

uncoated, 470 nm

0.1	0.5	0.1
0.7	CP	1.1
0.1	0.7	0.2

coated, 470 nm

0.1	0.6	0.1
0.9	CP	0.8
0.1	0.7	0.1

3.6. Usage of WLS films in a RICH detector

In the following, the results of an in-beam test of the coated and uncoated MAPMTs used in a prototype of the CBM-RICH detector are summarized with focus on Cherenkov ring hit multiplicity and ring sharpness.

(a) Cherenkov ring hit multiplicity – Fig. 9 shows integrated Cherenkov rings detected without (left) and with WLS film (right). An increased hit multiplicity for WLS coated MAPMTs is observed. For a quantitative analysis, Gaussian functions were fit to the hit multiplicity distributions with and without WLS film (least squares fit) and the mean of the fits are compared. This is shown exemplarily in Fig. 10 for H8500D-03 MAPMTs, for which an increase in hit multiplicity by 18% was observed.

The different types of MAPMTs compare as follows: The gain due to WLS films is (21.2 ± 1.4)% for rings detected by H10966A-103 MAPMTs, (18.2 ± 1.5)% for H8500D-03, and (18.0 ± 1.4)% for R11265-103-M16. These results are compatible with the hierarchy of relative *QE* gain shown in Fig. 6 (bottom).

Furthermore, the experimental results agree well with a full Monte Carlo simulation of the experimental setup using the measured *QE* curves for the different MAPMT types (Table 3, [17]). The precision of the experimentally determined hit multiplicity given in the table is obtained by monitoring the detector performance under stable conditions. The uncertainty of the

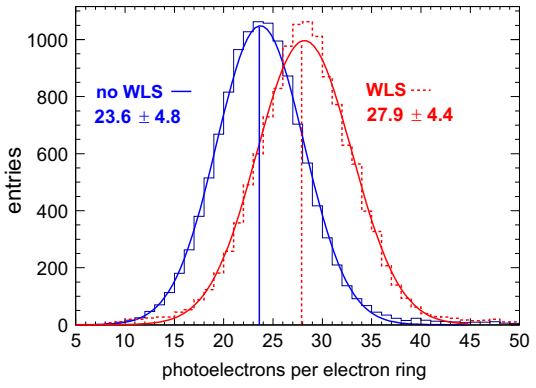

Fig. 10. Hit multiplicity distribution measured with H8500D-03 MAPMTs with dip-coated WLS films of ≈ 200 nm thickness in comparison to the same MAPMTs after film removal. The numbers indicate mean and sigma of the Gaussian fits to the data. Although the peak region of the WLS covered MAPMTs is not perfectly reproduced, mean value and width of the fitted distributions compare well with the data.

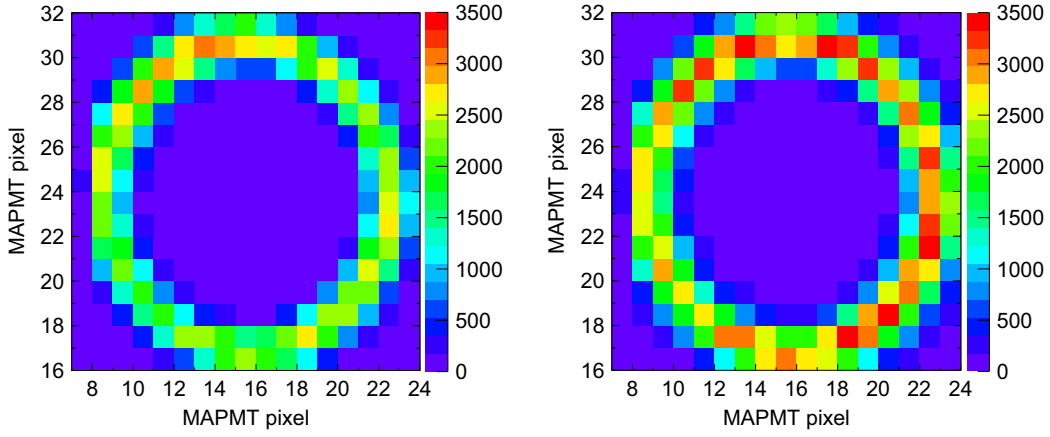

Fig. 9. Integrated Cherenkov rings from 10,000 electrons detected with the CBM RICH prototype. The ring radius is approximately 45 mm so that a ring covers an array of two by two MAPMTs of 5.8×5.8 cm^2 each. The left plot shows the number of hits per MAPMT pixel without WLS film, the right plot shows the number of hits with WLS film. A correction for radiator pressure and temperature was applied. An increased hit multiplicity with WLS film is observed.

Table 3
Comparison of experimentally observed and simulated increase of hit multiplicity $\Delta N/N$ due to the usage of WLS films during the in-beam test with the CBM RICH prototype at the CERN PS.

MAPMT type	$\Delta N/N$ experiment	$\Delta N/N$ simulation
R11265-103-M16	$(18.0 \pm 1.4)\%$	$(14.8 \pm 3.9)\%$
H8500D-03	$(18.2 \pm 1.5)\%$	$(18.3 \pm 4.7)\%$
H10966A-103	$(21.2 \pm 1.4)\%$	$(23.1 \pm 4.3)\%$

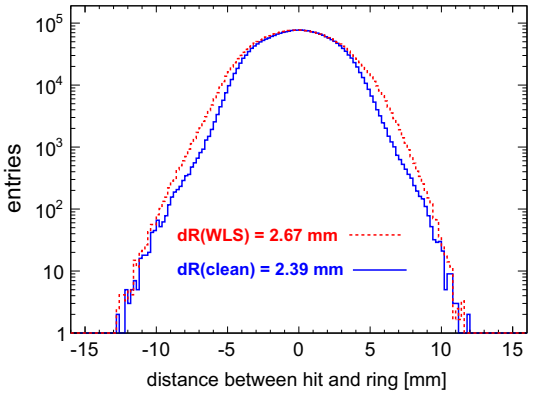

Fig. 11. Distribution of the distance between each hit and the ring fit for WLS coated and uncoated ring positions. The parameter *dR* is defined as the *RMS* of this distribution and is a measure of the ring sharpness. It can be seen that the ring sharpness decreases measurably when using WLS films. However, compared to the limited spatial resolution given by the MAPMT pixel size of $5.8 \times 5.8\ \mathrm{mm}^2$, the increase of *dR* by 0.3 mm is negligible.

results from Monte Carlo simulations is mainly determined by the extrapolation of the measured *QE* curves from 200 nm to 180 nm.

(b) Ring sharpness – Due to the isotropic fluorescence of WLS films, the Cherenkov ring sharpness is expected to decrease when using WLS coated MAPMTs. In addition, chromatic dispersion, which is stronger towards shorter wavelengths [18], may lead to a reduced ring sharpness when being more sensitive to UV photons. The ring sharpness is quantified by the parameter *dR*, which is the RMS of the distribution of the distance between each hit and the ring fit. Fig. 11 shows such distributions for a total of $\approx 2.5 \times 10^6$ Cherenkov rings. The parameter *dR* increases by 0.3 mm for WLS coated MAPMTs, which corresponds to a respective decrease of ring sharpness. This, however, is not significant compared to the spatial resolution of the MAPMTs which is determined by the pixel size, i. e. $5.8\ \mathrm{mm}/\sqrt{12} = 1.7\ \mathrm{mm}$.

4. Conclusion

We investigated the effect of dip-coated WLS films on MAPMTs with UV-extended windows with respect to *QE*, homogeneity, and crosstalk of the MAPMTs, as well as their performance in a prototype RICH detector. With dip-coated WLS layers of ≈ 180 nm, a significant increase of *QE* was achieved in the lower wavelength region (≤ 280 nm) without decrease of *QE* for $\lambda \geq 280$ nm. The increase in *QE* depends on MAPMT window thickness and photocathode material. The WLS films are more efficient on thick windows compared to thin windows and are more efficient on MAPMTs with SBA photocathodes compared to those with BA photcathodes. The homogeneity of the signal of PMTs with WLS film was found to be comparable to the homogeneity of PMTs without WLS film. An increase in crosstalk was observed for MAPMTs with WLS films. However, the effect is small and the Cherenkov ring resolution was not significantly affected for MAPMTs with WLS films when operated in a gaseous RICH detector. Thus, we can also exclude that an increase in chromatic dispersion due to the higher sensitivity to UV photons leads to a significant loss of ring resolution. On the other hand, the WLS films led to a significant increase of the number of detected photons in our RICH prototype: depending on the used MAPMT type, the photon yield is larger by 18%–21% compared to uncoated MAPMTs. Thus, we conclude that WLS films applied by means of dip-coating can be advantageously used on MAPMTs with UV-extended windows.

Acknowledgements

This work was supported by the Hessian LOEWE initiative through the Helmholtz International Center for FAIR (HIC for FAIR), by the GSI F&E-Cooperation with Giessen and Wuppertal (WKAMPE1012), by BMBF Grants 05P12RGFCG, 05P12PXFCE, and 05P09PXFC5, by the National Research Foundation of Korea (2012004024), by Helmholtz Grant IK-RU-002, and by SC ROSATOM through FRRC. We also thank C. Joram and A. Braem from CERN, P. Koczon from GSI, and T. Schweizer from Hochschule Esslingen for valuable contributions in the early stage of the experiments, as well as J. Kraut (Hochschule Esslingen) for taking the SEM images.

References

[1] E. Wagner, et al. (Eds.), Sensors, A Comprehensive Survey, Optical Sensors, vol. 6, Wiley-VCH, 1991.
[2] K.K. Hamamatsu Photonics, Photomultiplier Tubes, Basics and Applications, World Technical Writing, Hamamatsu, Japan, 2002.
[3] M. Ogawa, Journal of Chemical Physics 54 (1971) 2550.
[4] C. Höhne, et al., Nuclear Instruments and Methods in Physics Research Section A 595 (2008) 187.
[5] J. Adamczewski-Musch, et al., Nuclear Instruments and Methods in Physics Research Section A 766 (2014) 101.
[6] E.L. Garwin, Y. Tomkiewicz, D. Trines, Nuclear Instruments and Methods 107 (1973) 365.
[7] P. Baillon, et al., Nuclear Instruments and Methods 126 (1975) 13.
[8] G. Eigen, E. Lorenz, Nuclear Instruments and Methods 166 (1979) 165.
[9] M.A.F. Alves, et al., Nuclear Instruments and Methods 119 (1974) 485.
[10] A.M. Gorin, et al., Nuclear Instruments and Methods in Physics Research Section A 251 (1986) 461.
[11] D. Paneque, H.J. Gebauer, E. Lorenz, R. Mirzoyan, Nuclear Instruments and Methods in Physics Research Section A 518 (2004) 619.
[12] V. Körstgens, et al., Applied Physics Letters 93 (2008) 041916.
[13] S. Selvakumar, K. Sivaji, A. Arulchakkaravarthi, S. Sankar, Materials Letters 61 (2007) 4718.
[14] C. Höhne, et al., Nuclear Instruments and Methods in Physics Research Section A 639 (2011) 294.
[15] O. Chiantore, M. Lazzari, Polymer 42 (2001) 17.
[16] J. Adamczewski-Musch, et al., Nuclear Instruments and Methods in Physics Research Section A 766 (2014) 180.
[17] J. Kopfer, Dissertation, Bergische Universität Wuppertal, 2014.
[18] A. Bideau-Mehu, et al., Optics Communications 9 (1973) 432.